MECHANICAL PROPERTIES OF REDUCED GRAPHENE OXIDE POLYMER COMPOSITES

Peng Xu and Balaji Panchapakesan

Small Systems Laboratory
Department of Mechanical Engineering
University of Louisville, Louisville, KY 40292; b0panc01@louisville.edu

ABSTRACT

In this paper, mechanical properties of chemically derived single layer graphene oxide as reinforcements in poly (dimethyl) siloxane (PDMS) macroscopic composites is reported. A Raman G mode shift of 11.2 cm^{-1}/% strain in compression and 4.2 cm^{-1}/% strain in tension is reported suggesting high load transfer. An increase in elastic modulus of PDMS by ~42%, toughness by ~39%, damping capability by ~673%, and strain energy density of ~43% by the addition of 1 wt. % reduced graphene oxide in PDMS is reported.

1 INTRODUCTION

Defect free sheets of graphen exfoliated mechanically from graphite flakes was measured to have second order elastic stiffness of 340 N/m, breaking strength of 42 N/m and Young's modulus of 1.0 Tpa [1]. Such excellent mechanical properties of exfoliated graphene warrant their investigation as fillers in advanced polymer composites. Recently, interfacial stress transfer of exfoliated graphene transferred on top of polymer substrate was demonstrated using Raman spectroscopy [2, 3]. Significant shift in the Raman G' or 2D bands (> -50 cm^{-1}/% strain) were observed, demonstrating load transfer to the carbon layer [2, 3]. Several studies on exfoliated graphite based polymer composites have shown enhanced mechanical strength, toughness, glass transition temperature, increase in electrical conductivity and gas barrier properties [4-11]. The work by Coleman *et al*., is notable as it yielded a ~100 times increase in elastic modulus at 3% strains for 50 wt. % exfoliated graphene drop casted in polyurethane [11]. While these studies are impressive reiterating the importance of graphene as filler materials in polymer composites, current methods of fabrication of advanced polymer composites using mechanically exfoliated graphene are quite limited. This is due to the fact that yield of mechanically exfoliated graphene at present is limited to 1 wt.% which could be increased to 7-12% with additional processing [12]. In this context, the use of chemically reduced graphene oxide (RGO) as fillers in polymer composites becomes important and warrants investigation for development of low cost and high strength advanced composites. Graphene sheets chemically derived from graphene oxide using Hummer's method and subsequent reduction by hydrogen plasma has been heralded as one of the methods for large scale production of graphene suitable for industrial use [13]. Microscopic characterization of such graphene sheets has shown large unoxidized graphitic regions in between defective clusters and therefore could witness interesting mechanical properties [14]. Recent studies have shown that despite the defects in their lattice, such sheets have shown extraordinary stiffness with Young's modulus E=0.25 TPa, approaching that of pristine graphene, with high flexibility and lower built-in tension [13]. Therefore, studying the interfacial load transfer and mechanical properties of reduced graphene sheets in polymers can make progress in the area of low cost, high strength and scalable composites based on graphene.

Over the years Raman spectroscopy has become a powerful tool to understand interfacial load transfer in carbon fibers and nano-carbon fillers such as carbon nanotubes in polymer composites [15, 16]. The disorder induced 2D bands and tangential mode G band has been demonstrated to be sensitive to both compressive and tensile strains in nano-carbon fillers such as carbon nanotubes [15, 16]. The Raman stress sensitivity arises from the anharmonicity of the atomic bonds [17]. By using the interatomic potentials of the harmonic bond model and including the attractive and repulsive contributions (Mie and Gruneisen parameters), past theoretical framework has demonstrated a direct relationship between the wavenumber shift in the Raman bands and bond deformation which can be expressed mathematically as: $\bar{w} = \bar{w}_0\left[1-\left(\frac{a+r+3}{2}\right)\times\varepsilon_L\right]$, where, a and r are positive constants depending on the bond type and ε_L is the strain applied [17]. Therefore, the strain induced Raman band shifts is a measure of the change in interatomic distances or bond deformation due to the load transferred from the polymer to the graphene fillers. The eventual mechanical properties of the composites are bound to depend on the extent to which the load is transferred from the polymer to the graphene filler and the graphene/polymer interface should play the most important role in efficient stress transfer. Larger the shift in Raman wavenumbers is therefore as a result of higher stress transfer from the polymer to the graphene fillers and can be mathematically expressed using the following equation:

$\Delta\sigma = E_f \varepsilon_L = -\frac{E_f \cdot \Delta\overline{w}}{R(a,r)}$, where E_f is the young's modulus of filler material, and Δw wavenumber shift. Therefore, if the filler has the same bond type and assuming that the applied strain field is constant throughout the composite matrix, the larger the Raman wavenumber shift means higher load transfer.

2 EXPERIMENTAL

Commercially obtained RGO (92% carbon, <8% oxygen) produced via thermal exfoliation reduction and hydrogen reduction of single layer graphene oxide) was purchased from ACS Materials. The RGO was used in its original form and not surface modified at any time. GNPs were purchased from ACS Materials and were prepared by plasma exfoliation with >99% purity and ~3-5 layers. The number of layers were verified using SEM and was characterized in the past using layer dependent shifts in Raman spectroscopy [18]. Sylgard 184 silicone elastomer (Fisher Scientific) was chosen as the matrix because it is commonly used in industrial/scientific research and biocompatible. The term 'wt%' used throughout the paper refers to the ratio of carbon additive to PDMS base compound. Homogenous dispersion of graphene (1 wt. % of RGO and GNP for comparison) in PDMS was prepared using a shear mixing process. SEM imaging was conducted on a Zeiss SUPRA 35VP field emission scanning electron microscope. The ~632.8 nm line beam of a helium-neon laser in an inVia RENISHAW micro-Raman spectrometer was focused onto the sample surface through a ×50 objective lens, forming a laser spot approximately 3 μm in diameter. Samples containing 1 wt. % RGO or GNP in PDMS were prepared and tested for their elastic modulus until failure. Stress-strain curves and cyclic stress-strain curves were measured using a Rheometric Mechanical Analyzer (RMA, TA instruments-Waters LLC) for both RGO and GNP composites. Cyclic mechanical testing was conducted on 10 samples for each RGO/PDMS sample to investigate stress-strain curves, toughness and strain energy density of the composites. For more details on the experimental details, the reader is asked to consult reference [19]

3 RESULTS AND DISCUSSION

Figure 1 (a-1) presents an SEM image of GNPs, which are comprised of 3-5 graphitic layers [18]. Figure 1 (a-2) presents an SEM image of GNP/PDMS composite. One can see that the rigid stack like morphology of GNP is maintained in the polymer matrix. Figure 1 (b-1) presents an SEM of RGO. Figure 1 (b-2) presents an SEM image of RGO/PDMS composite. GNPs show a rigid stack/plate like morphology while RGO demonstrate morphology of thin ribbon but with excellent dispersion.

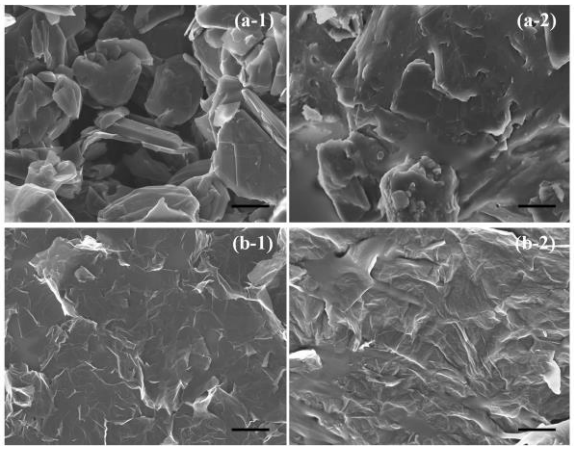

Figure 1: SEM images: (a-1) GNPs; (a-2) GNP/PDMS; (b-1) RGO; (b-2) RGO/PDMS; Scale bar: 1 μm in all the images.

Figure 2 (a) presents the G mode shift of GNP/PDMS with application of both tensile and compressive strains. For GNP/PDMS composites, rate of peak shift with strain was ~2.4 cm^{-1}/% strain in tension and ~1.2 cm^{-1}/% strain under compression as shown in Figure 2(b) and rate of peak shift is similar to the earlier report [20]. In addition, we also measured the 2D band shifts that were quantified to be ~0.8 cm^{-1}/% strain under tension and ~0.7 cm^{-1}/% strain under compression, which was smaller than G band, however demonstrating use of 2D band shift in GNP fillers for measuring load transfer. On the contrary, the 2D bands were the most sensitive to strains in carbon nanotubes where 6 cm^{-1}/% was witnessed in tension in our past work for the same process conditions [21]. Based on the G-band Raman shift, the interfacial stress was calculated to be ~80 GPa for the GNP/polymer interface in compression. For RGO/PDMS, rate of G-peak shift with strain was ~4.4 cm^{-1}/% strain in tension and ~11.2 cm^{-1}/% strain in compression suggesting enhanced load transfer in compression in bulk. The interfacial stress was calculated to be ~410 GPa for RGO interface suggesting fivefold increase in stress transfer in compression. For tension, the load transfer of RGO polymer interface was calculated to be ~3.5 times that of GNP interface. This also suggest greater load transfer of RGO compared to single wall nanotube fillers in tension [20]. Enhanced load transfer was witnessed for RGO fillers in both tension and compression compared to GNP fillers (Figure 2 (c)). Such large Raman shifts suggest large bond deformation, minimum slippage that must originate only from intimate contact of the RGO with the polymer and better dispersion through long mixing. Comparing this to past report on nanotube composites have only demonstrated either large Raman peak shift (15 cm^{-1} of 2D band) in compression and small peak shift in tension [22].

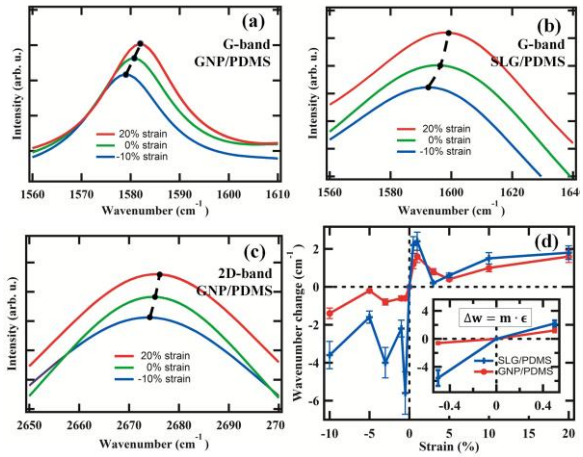

Figure 2: Load transfer: (a) G band shift in GNP/PDMS, (b) G-band shift in RGO/PDMS, (c) 2D band shift of GNP/PDMS, (d) change in Raman wavenumbers with strains.

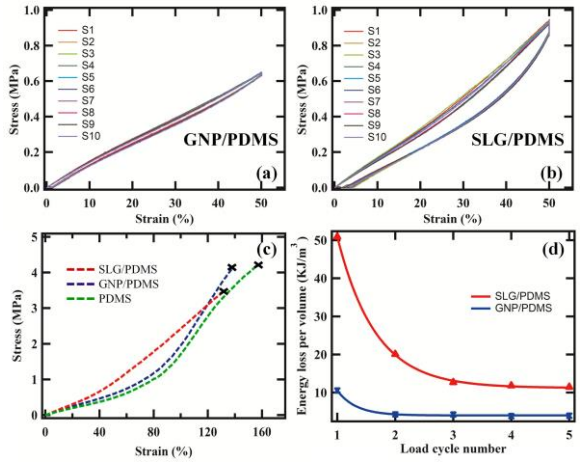

Figure 3: Mechanical Properties: cyclic stress-strain curves of (a) GNP/PDMS, (b) RGO/PDMS, (c) stress-strain curve of all the composites tested till failure, (d) energy loss with cycling.

Figure 3 (a-b) presents the cyclic stress-strain curves of both the composite samples with from 10 different repeats (different samples) marked S1-S10. The area under the hysteresis curve represents energy loss during the loading and unloading cycles. The area under the hysteresis curve is larger for RGO/PDMS indicating 673% improvement in damping capability compared to pure PDMS. On the other hand, area under the hysteresis loop was smaller for GNP/PDMS matrix ~139% the area for pure PDMS. The large damping capability of RGO fillers demonstrate considerable interfacial slippage between the PDMS and fillers and high thermal conductivity [23]. This brings in an interesting question of whether the orientation of the graphene with respect to the longitudinal or transverse loading can affect energy dissipation and could serve as useful design parameter for future composites and is worth investigating in future. Figure 3 (c) presents the stress-strain curve of GNP/PDMS, RGO/PDMS and pure PDMS samples till failure. As more strain is applied, the polymeric chains in PDMS are stretched out till final failure was seen ~160%. RGO/PDMS samples exhibited a linear stress-strain curve with failure at ~120%, almost 25% lower failure strains. This suggests considerable stiffening of the matrix with addition of RGO at these low weight percentages. The increase in elastic modulus for RGO/PDMS was ~42% while that of GNP/PDMS was ~30%. Figure 3 (d) presents the calculated energy loss for RGO/PDMS and GNP/PDMS composites. An energy release of ~50.9 kJ/m^3 for one cycle and lowering as the cycles are repeated. The frictional energy due to RGO interacting with the polymer on loading and recovery during unloading is clearly represented in these cycles. At the fifth cycle, the energy loss is saturated at ~11.4 kJ/m^3. However, GNP/PDMS show five time small energy loss at ~10.6 kJ/m^3 at first cycle and saturating quickly to ~3.8 kJ/m^3 from the second to the fifth cycle. The energy loss shows that slippage and friction between polymer and filler can be tuned in RGO based composites to much higher level than GNPs. Investigating further, the area under the stress-strain curve also represents toughness. This was calculated at 1.92 MJ/m^3 for RGO/PDMS, 1.59 MJ/m^3 for GNP/PDMS and 1.38 MJ/m^3 for pure PDMS at 130% end point strain. The flexibility of RGO can result in large energy absorption without failing resulting in increased toughness of the composite. Finally, energy density values were calculated as ~1.87 kJ/Kg for RGO/PDMS, ~1.52 kJ/Kg for GNP/PDMS and ~1.30 kJ/Kg for pure PDMS. This suggests an increase in strain energy density of ~43% for RGO fillers in PDMS. The high surface area of RGO sheets makes the intimate interaction with the polymer due to increased adhesion resulting in higher strain energy densities [24]. In the elastic regime, these high densities can be recovered as useful mechanical work thereby making RGO highly attractive for realization of advanced composites.

4. CONCLUSIONS

RGO in PDMS showed enhanced load transfer, mechanical strength, damping capability, strain energy sensitivity and elastic modulus compared to their GNP counterparts. It is seen that the failure mechanisms of RGO in PDMS are quite different from those of GNPs which needs further investigation. A Raman G mode shift of 11.2 cm^{-1}/% strain in compression and 4.2 cm^{-1}/% strain in tension is reported suggesting enhanced load transfer in compression. An increase in elastic modulus of PDMS by ~42%, toughness by ~39%, damping capability by ~673%, and strain energy density of ~43% by the addition of 1 wt. % RGO in PDMS is reported. Such excellent mechanical property improvement for small fraction of chemically derived RGO presents opportunities for developing low cost advanced composites based on graphene.

REFERENCES

1. Lee, C., et al., Science, 2008. 321(5887): p. 385-388.
2. Gong, L., et al., Advanced Materials, 2010. 22(24): p. 2694-+.
3. Young, R.J., et al.. Acs Nano, 2011. 5(4): p. 3079-3084.
4. Song, P.G., et al, Polymer, 2011. 52(18): p. 4001-4010.
5. El Achaby, M., et al., Polymer Composites, 2012. 33(5): p. 733-744.
6. Kalaitzidou, K., H. Fukushima, and L.T. Drzal, Composites Part a-Applied Science and Manufacturing, 2007. 38(7): p. 1675-1682.
7. Wakabayashi, K., et al., Polymer, 2010. 51(23): p. 5525-5531.
8. Raghu, A.V., et al., Macromolecular Chemistry and Physics, 2008. 209(24): p. 2487-2493.
9. Nguyen, D.A., et al., Polymer International, 2009. 58(4): p. 412-417.
10. Kim, H., Y. Miura, and C.W. Macosko, Chemistry of Materials, 2010. 22(11): p. 3441-3450.
11. Khan, U., et al., Carbon, 2010. 48(14): p. 4035-4041.
12. Hernandez, Y., et al., Nature Nanotechnology, 2008. 3(9): p. 563-568.
13. Gomez-Navarro, C., M. Burghard, and K. Kern, Nano Letters, 2008. 8(7): p. 2045-2049.
14. Lerf, A., et al., Journal of Physical Chemistry B, 1998. 102(23): p. 4477-4482.
15. Schadler, L.S., S.C. Giannaris, and P.M. Ajayan, Applied Physics Letters, 1998. 73(26): p. 3842-3844.
16. Mu, M.F., et al., Nanotechnology, 2009. 20(33).
17. Gouadec, G. and P. Colomban, Progress in Crystal Growth and Characterization of Materials, 2007. 53(1): p. 1-56.
18. Loomis, J., B. King, and B. Panchapakesan, Applied Physics Letters, 2012. 100(7).
19. Xu, P., et al., Nanotechnology, 2012. 23(50).
20. Srivastava, I., et al., Applied Physics Letters, 2011. 98(6).
21. Xu, P., J. Loomis, and B. Panchapakesan, Applied Physics Letters, 2012. 100(13).
22. Ajayan, P.M., et al., Advanced Materials, 2000. 12(10): p. 750-+.
23. Ci, L., et al., Nano Letters, 2008. 8(9): p. 2762-2766.
24. El-Lawindy, A.M.Y. and S.B. El-Guiziri, Journal of Physics D-Applied Physics, 2000. 33(15): p. 1894-1901.

ACKNOWLEDGEMENTS

Funding for this work was partially supported by ECCS: 1202190, and CMMI: 1233996 for Balaji Panchapakesan